ISPRS Journal of Photogrammetry and Remote Sensing 85 (2013) 93–101

Contents lists available at ScienceDirect

ISPRS Journal of Photogrammetry and Remote Sensing

journal homepage: www.elsevier.com/locate/isprsjprs

Diurnal and seasonal impacts of urbanization on the urban thermal environment: A case study of Beijing using MODIS data

Zhi Qiao, Guangjin Tian *, Lin Xiao

State Key Laboratory of Water Environment Simulation, School of Environment, Beijing Normal University, No. 19, Xinjiekouwai Street, Beijing 100875, PR China

ARTICLE INFO

Article history:
Received 23 May 2013
Received in revised form 23 August 2013
Accepted 25 August 2013
Available online 21 September 2013

Keywords:
Urbanization
Land surface temperature
Contribution index
MODIS
Beijing

ABSTRACT

Beijing has experienced rapid urbanization and associated urban heat island effects and air pollution. In this study, a contribution index was proposed to explore the effect of urbanization on land surface temperature (LST) using Moderate-Resolution Imaging Spectroradiometer (MODIS)-derived data with high temporal resolution. The analysis indicated that different zones and landscapes make diurnally and seasonally different contributions to the regional thermal environment. The differences in contributions by the three main functional zones resulted from differences in their landscape compositions. The roles of landscapes in this process varied diurnally and seasonally. Urban land was the most important contributor to increases in regional LSTs. The contributions of cropland and forest varied distinctly between daytime and nighttime owing to differences in their thermal inertias. Vegetation had a notable cooling effect as the normalized vegetation difference index (NDVI) increased during summer. However, when the NDVI reached a certain value, the nighttime LST shifted markedly in other seasons. The results suggest that urban design based on vegetation partitions would be effective for regulating the thermal environment.

© 2013 International Society for Photogrammetry and Remote Sensing, Inc. (ISPRS) Published by Elsevier B.V. All rights reserved.

1. Introduction

Urbanization has improved various aspects of human living conditions (Rizwan et al., 2008). At the same time, however, environmental problems resulting from urbanization (e.g., global warming, air pollution, and environmental deterioration) have negatively affected the quality and comfort of urban living. The urban population is forecast to reach five billion by 2030 (Ash et al., 2008), and land surfaces will be severely altered as large numbers of people migrate into metropolitan areas (Wang et al., 2007). Urbanization has become a major cause of environmental problems (Chen et al., 2006).

The change from non-urban to urban land uses can result in climate changes in urban areas, and land surface temperature (LST) change has been a key area of urban climate research (Voogt and Oke, 2003). Distinct differences between urban areas and surrounding rural areas have been widely observed, a phenomenon termed the urban heat island (UHI) effect (Oke, 1982; Gallo et al., 1993). Studies of UHIs have often cited urban size as a main factor in the UHI development (Oke, 1973). In addition, increased population density is linked to higher anthropogenic heat release, including heat releases from power plants, vehicles, building materials, and air conditioners (Oke, 1988; Christen and Voogt, 2004; Rizwan et al., 2008). Furthermore, urban temperature will increase as human-made structures and impervious surfaces replace vegetation, greenery, and water, which would otherwise lower the LST (Yuan and Bauer, 2007). A complicated urban surface also absorbs and stores large amounts of solar shortwave radiation (Wang et al., 2007), while the reduction of sky-view factors decreases the loss of longwave radiation (Oke, 1988; Rizwan et al., 2008). Furthermore, the roughness of structures reduces the amount of convective heat removal because it lowers wind speeds (Christen and Voogt, 2004). More importantly, declines in thermal inertia and the vegetation index constrain evaporation, consequently reducing the loss of heat by latent heat flux (Kondoh and Nishiyama, 2000). Air pollutants also play a role in UHI formation (Rizwan et al., 2008). In summary, an UHI is a response to complex energy and water balances, as well as air movement (Oke, 1988; Voogt and Oke, 2003; Chen et al., 2006).

Statistical studies using meteorological data, remote sensing technology, and physical modeling have confirmed that urbanization contributes to global warming in various ways (Wood, 1988; Jones et al., 1990; Kalnay and Cai, 2003; Parker, 2004; Chen et al., 2006; Trusilova et al., 2008; Xu, 2009). Conditions in surrounding rural areas also affect the magnitude of an UHI (Hawkins et al., 2004). For example, Streutker (2002) found that UHI intensity was inversely correlated with rural LST. However, simply

* Corresponding author. Tel.: +86 10 58807808; fax: +86 10 58800397.
E-mail address: tianguangjin@gmail.com (G. Tian).

0924-2716/$ - see front matter © 2013 International Society for Photogrammetry and Remote Sensing, Inc. (ISPRS) Published by Elsevier B.V. All rights reserved.
http://dx.doi.org/10.1016/j.isprsjprs.2013.08.010

comparing the difference in LST between urban land and the surrounding rural area is not an effective method to quantify the intensity of the UHI (Xu, 2009). Quantitative studies of the relationship between land use/cover patterns and LST, with regard to LST variations in areas undergoing urbanization, can help to clarify the mechanisms that create the UHI and provide a quantitative measurement of the contribution of urbanization to the UHI effect over time.

Satellite observation provides a quantitative measurement of urban sprawl and LST. Remote sensing data are also advantageous for exploring the role of the surface energy budget in the UHI (Wang et al., 2007). Since Rao (1972) demonstrated that satellite images can be applied to retrieve the thermal footprints of urban areas, satellite data have been used to study LST and the UHI, with many studies using Advanced Very High Resolution Radiometer (AVHRR) data from the National Oceanic and Atmospheric Administration (NOAA) (Gallo and Owen, 1998; Streutker, 2002). Thermal infrared (TIR) data from the Thematic Mapper (TM) and Enhanced Thematic Mapper Plus (ETM) have also been utilized to study the UHI effect (Weng, 2001; Nichol and Wong, 2005). The present study analyzed Terra/Moderate-Resolution Imaging Spectroradiometer (MODIS) LST products collected in 2008. In addition, Landsat TM images were analyzed to retrieve land use types. The study focused on the following: (1) quantitatively calculating the contributions of various functional zones and land use/cover patterns to the thermal environment in the Beijing metropolitan region; (2) exploring the effect of the thermal environment based on an analysis of the temporal-spatial contributions of different landscapes; and (3) verifying the reliability of the contributions of different landscapes to the regional thermal environment through quantitative evaluations of LST–normalized difference vegetation index (NDVI) relationships.

2. Data

MODIS is a crucial instrument aboard NASA's Terra (formerly, Earth Observing System [EOS] AM) and Aqua (EOS PM) satellites for global studies of atmosphere, land, and ocean processes. Terra was launched on 18 December 1999, and its overpass times are around 1030 (local solar time) in its descending mode and 2230 local solar time in its ascending mode. MODIS Version 5 global land products were used in this study (8-day LST/emissivity L3 Global 1000 m SIN Grid (MOD11A2)) (Friedl et al., 2010).

The MODIS LST products have been widely used in investigations of the UHI effect (Jin et al., 2005; Hung et al., 2006; Pongracz et al., 2006). The split-window algorithm is used to retrieve LST by applying multiple bands from the thermal and middle infrared spectral bands of MODIS (Wan and Dozier, 1996). In addition, the products have been corrected for atmospheric effects and surface emissivity. The accuracy of the products has been verified to be approximately 1 K of the root mean-square error (Wan et al., 2004). Considering possible alternatives, such as TM/ETM or Advanced Spaceborne Thermal Emission and Reflection Radiometer (ASTER) products, the MODIS LST products have a relatively low resolution (1 km). However, more images are available from MODIS than from these alternatives because of MODIS's high temporal resolution. Twice-daily MODIS data can be obtained free of charge from http://lpdaac.usgs.gov. Because of the abundant noise from cloud cover and snow, this study used the eight-day LST/emissivity product (MOD11A2) to diminish the influence of noise when retrieving LST (Rajasekar and Weng, 2009). The eight-day LST/emissivity products (MOD11A2) are composed of daily 1-km LST products (MOD11A1) and are calculated as the average value of clear-sky LSTs during an eight-day period. To avoid the effects of clouds, eight high-quality images on 22 April, 19 July, 7 October, and 2 December 2008 were selected to be representative of spring, summer, autumn, and winter, respectively. We selected these eight images because of their relatively high quality, as indicated by the attached quality control (QC) files. In addition, data from two national meteorological stations (Beijing station and Miyun station) in the Beijing metropolitan region (Fig. 1) were used to supplement the selected images. The station records include maximum air temperature, minimum air temperature, precipitation, wind speed, and wind direction.

The MODIS bidirectional reflectance distribution function (BRDF)/albedo products can characterize the anisotropic reflectivity of the land surface (Schaaf et al., 2002). The albedo products have been confirmed to have a good level of accuracy, with a root mean-square error of approximately 0.02 (absolute value), when compared with field measurements (Lucht et al., 2000; Liang et al., 2002; Wang et al., 2004).

The MODIS global vegetation indices products include the NDVI and the enhanced vegetation index (EVI). The calculation of these indices involves the use of a filter based on quality, cloud cover, and viewing geometry, and thus the best quality pixels from all observations can be collected (van Leeuwen et al., 1999).

To retrieve the land cover types, Landsat TM images were chosen and radiantly corrected. The images were false-color composed of five, four, and three bands using the red–green–blue (RGB) method of artificial visual interpretation. There were six aggregated classes of land use: cropland, forest, grassland, water bodies, built-up land, and bare land. These classes were further divided into 25 land-use classes. The built-up land contains urban land, rural residential land, and industrial and mining sites. The average interpretation accuracies were 92.9% for land use and 97.6% for the detection of changes in land cover. For cropland, the accuracy was

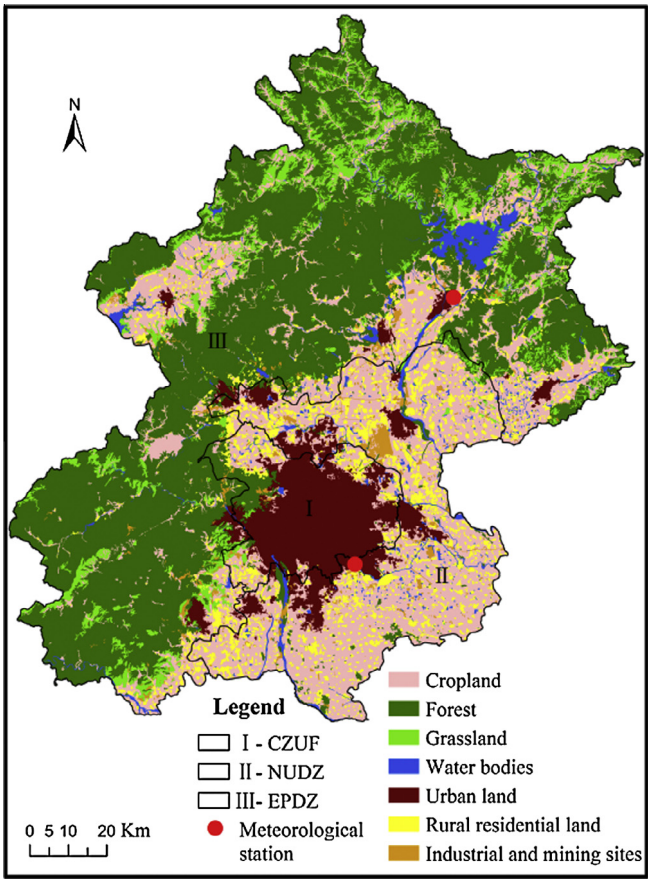

Fig. 1. Functional zones and landscapes in the Beijing metropolitan region.

94.9%. The built-up area had the highest accuracy of 96.3%. For forest and grassland, the accuracies were 90.1% and 88.1%, respectively (Liu et al., 2005). The land use dataset was provided by the Institute of Geographical Sciences and Natural Resources Research, Chinese Academy of Sciences.

3. Study area

Beijing is the capital of the People's Republic of China and extends approximately 1°37′ latitudinally (39°26′–41°03′ N) and 2°05′ longitudinally (115°25′–117°30′ E). It covers 14 districts and two counties, and the total urban area is approximately 16410.54 km^2 (Beijing Statistics Bureau, 2010). The urban area is surrounded by high mountains in its west and north with heights of 1000–1500 m. Plains cover 6390.3 km^2 in the eastern and southern parts of the Beijing metropolitan region. The city has a sub-humid warm temperate continental monsoon climate and four distinct seasons, with a cold and windy winter, and a hot and humid summer. However, environmental problems in Beijing have drawn international attention. The area experiences sand and dust storms in spring, the formation of an UHI in summer, and pollution haze in winter, all of which result from combinations of the terrain, location, ventilation, pollution sources, and urbanization (Xia et al., 2006).

With the development of remote sensing technology and field observations, a large amount of research on the effects of the UHI in the Beijing metropolitan region have been undertaken in the past three decades. Distinct spatial patterns and seasonal variations have been described. Namely, the nighttime UHI intensity is relatively stable and the influence of land use/cover patterns on the UHI in the daytime is greater than in the nighttime. A negative UHI normally occurs in winter and spring (Wang et al., 2007). Zhang et al. (2005) reported that the average UHI was approximately 4–6 °C when using a suburban area in the northwestern region as the rural baseline and 8–10 °C when using the outer suburban area in the same region. With the diversified and rapid development of the economy and urban society, urban sprawl in Beijing will likely expand and the UHI effect will become more severe (Xu, 2009).

4. Methods

Urbanization can generate significant LST increases (Wood, 1988; Jones et al., 1990; Kalnay and Cai, 2003; Parker, 2004), resulting from the process of urban land encroaching on other landscapes that previously reduced the regional LST (Chen et al., 2006; Trusilova et al., 2008; Xu, 2009). However, each type of urban expansion pattern in different regions and even in different seasons makes a different contribution to the process (Chen et al., 2006). Xu (2009) presented three indices to evaluate the UHI intensity: source landscapes (industrial areas, commercial areas, airports, and residential areas), sink landscapes (vegetation, greenery and water), and the combined contribution of source and sink landscapes to the UHI intensity. The distinction between source landscapes and sink landscapes is based on whether they make positive contributions that increase the LST at a regional scale. This approach is highly valuable for spatially evaluating the contribution of each landscape to the UHI intensity.

In this study, the contribution of functional zones and landscapes to the urban thermal environment during the daytime and nighttime in various seasons was calculated. Considering the variations in LST and atmospheric conditions on the dates that the selected images were collected, we used the average differences in LST between the functional zone or landscape and the entire area rather than absolute LST changes. The proportions of the area of research objects were calculated initially (i.e., the proportions of functional zone in the entire area and the proportions of landscapes in each functional zone). The average LSTs of the research objects were recorded, including for the functional zones, landscapes, and the entire area. Finally, the contributions of the research objects to the urban thermal environment were defined as the products between the average LST difference and their proportion in the area (Chen et al., 2006). The contribution index (CI) was calculated as follows:

$$CI = D_t \times S \quad (1)$$

where CI is the contribution of the functional zone or landscape to the regional LST, D_t is the average LST difference between the functional zone or the landscape and the entire area, and S is the proportion of the area.

5. Results

5.1. Proportional areas of functional zones and landscapes

The land use/cover landscapes were retrieved through a visual interpretation of Landsat TM images. The areas of functional zones and landscapes were calculated and analyzed (Fig. 1).

According to the plan of Beijing's main-functional zone (2010–2020), the Beijing metropolitan region was divided into four functional zones: (1) The Core Zone of Capital Function, including the Dongcheng and Xicheng districts, which also have the highest level of complete urbanization. (2) The Urban Function Extended Zone, including the Haidian, Chaoyang, Fengtai, and Shijingshan districts, which have a relatively high level of urbanization but are not completely developed. To reduce the redundancy of the analysis, the two functional zones above were combined because each was small in area and their development objectives and functions were similar. The new combined zone was referred to as the Core Zone of Urban Function (I- CZUF). (3) The New Urban Development Zone (II- NUDZ), including Tongzhou, Shunyi, Daxing, and the plains in Fangshan and the Changping district, which have the largest development potential. (4) The Ecological Preservation Development Zone (III- EPDZ), including the Huairou, Pinggu, Mentougou districts, Miyun and Yanqing counties, and the mountains in Fangshan and the Changping district, which are the most important regions with regard to protecting ecosystems and water resource conservation.

The three functional zones differed significantly in size and land use compositions (Table 1). The proportions of each functional zone in the Beijing metropolitan region were 8.5%, 23.1%, and 68.4%, respectively. The level of urbanization decreased rapidly from the CZUF to EPDZ. Although only 8.5% of the total area, the CZUF had 60% of the permanent population and 70% of the GDP in the Beijing region according to Beijing's main-functional-zone plan (2010–2020). Urban land was the dominant landscape in the CZUF, accounting for 61% of the area in the zone. Cropland and forest made up 17.1% and 9.6%, respectively. Rural residential land was another important component of the CZUF, but was

Table 1
Areas of functional zones and landscapes.

Landscape	CZUF	NUDZ	EPDZ
Cropland	17.1	60.1	16.7
Forest	9.6	3.6	63.5
Grassland	1.0	0.7	11.4
Water bodies	1.5	4.3	2.9
Urban land	61.0	11.0	1.4
Rural residential land	7.8	16.6	3.0
Industrial and mining sites	2.0	3.7	1.1
The proportion of the zone	8.5	23.1	68.4

distributed in marginal areas of the zone. In the NUDZ, the main landscape was cropland, which accounted for 60.1% of the area of the zone. Urban land made up only 11% of the NUDZ, whereas rural residential land accounted for 16.6%. The permanent population was 27% of the city's total, and the GDP was 26% of the total. The EPDZ was the largest of the three functional zones, and vegetation was the dominant landscape, covering 91.5% of the total area. Forest was the largest landscape component, accounting for 63.5% of the total area, followed by cropland and grassland. Consequently, this zone had the lowest level of urbanization among the three functional zones. Urban land and rural residential land covered only 1.4% and 3.0% of the zone, respectively. The EPDZ had 13% of the total population and 4% of the GDP.

5.2. Contributions of the functional zones to the urban thermal environment

To explore the mechanisms of the regional thermal environment, the contributions of the three functional zones in the four seasons were calculated. Eight high-quality images on 22 April, 19 July, 7 October, and 2 December were selected to be representative of spring, summer, autumn, and winter, respectively. Fig. 2 illustrates the spatial pattern of LSTs in the summer in daytime.

Meteorological and MODIS LST data for the same period were compared. Despite many differences between the air temperature and LST, the results show a strong relationship between the two data types. The determination coefficients were 0.977 and 0.976 for Beijing station and Miyun station, respectively (Fig. 3). In addition, the average wind speed was less than 3.1 m/s, the maximum precipitation was only 4.3 mm, and there was no snow on the dates that the selected MODIS images were collected. This further confirms that the selected MODIS LST products were effective and receivable.

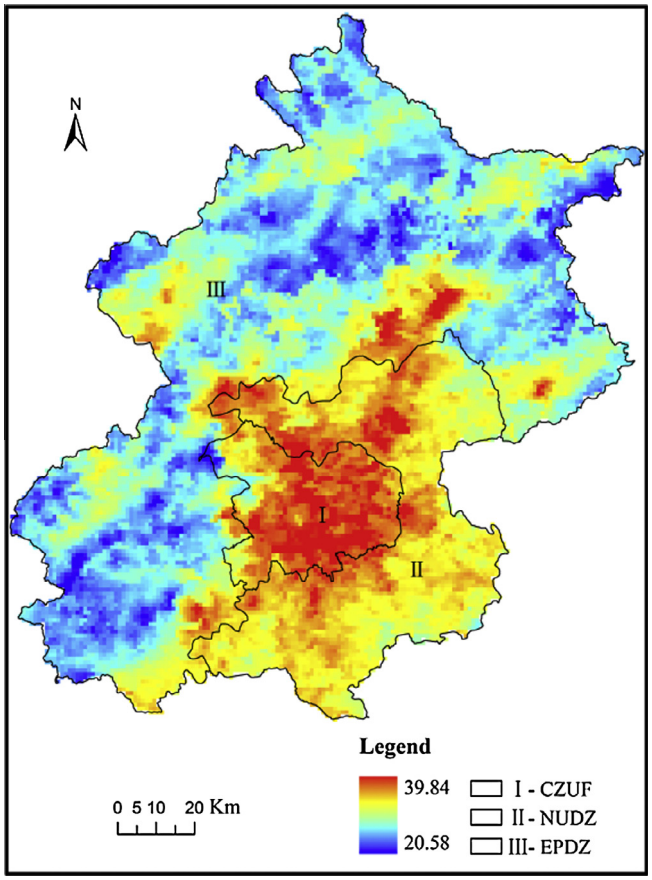

Fig. 2. Spatial pattern of land surface temperatures in summer in daytime.

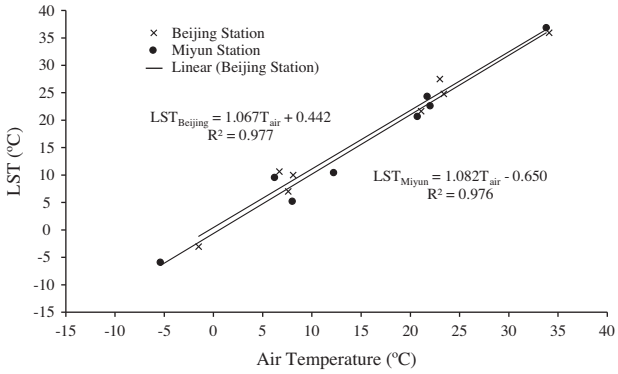

Fig. 3. The relationship between satellite-derived LST and air temperature measured at the meteorological stations.

First, the average LST differences between each functional zone and the Beijing metropolitan region were calculated and analyzed (Fig. 4).

The average LST of the two central regions (CZUF, NUDZ) were substantially higher than those for the entire region, whereas the LST of the EPDZ was lower than the LST of the whole region. Overall, the difference in LST was negative with distance from the urban center. The decline was particularly distinct in daytime in the summer and autumn. The largest difference reached 4.93 °C between the CZUF and the entire zone in the summer daytime. However, the average LST of the CZUF was not always significantly higher than that of the other zones. The LST of the CZUF was only 0.04 °C higher than that of the NUDZ in the winter daytime. The EPDZ LST was the lowest because of its flourishing vegetation and high elevation. In the EPDZ, the change in the LST was consistent with the growth of deciduous vegetation. The LST difference between the EPDZ and the whole Beijing metropolitan region reached a maximum in the summer daytime and a minimum in the winter nighttime. When comparing the difference during the daytime and nighttime, the LST was relatively stable in the nighttime. The impact of solar radiation was different because of the different thermal inertias of the landscapes in the daytime, whereas anthropogenic heat resources were relatively concentrated and stable during the nighttime.

Finally, the thermal environment contribution indices of the functional zones to the entire area were calculated for the daytime and nighttime in each of the four seasons (Table 2).

The thermal environment contribution index was defined as the product between the average LST difference and the proportion of the area. Therefore, the contribution index is positive with regard

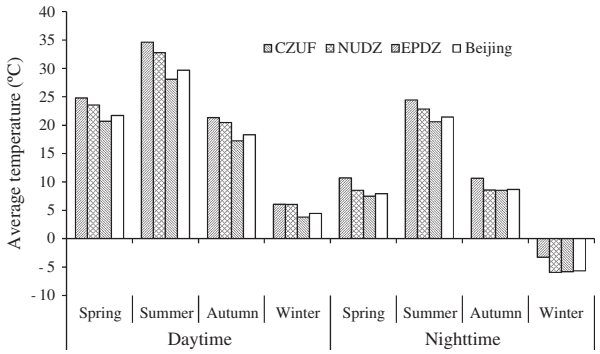

Fig. 4. Average LSTs of functional zones and the Beijing metropolitan region.

Table 2
Contributions of the functional zones to the urban thermal environment.

Zones	Daytime				Nighttime			
	Spring	Summer	Autumn	Winter	Spring	Summer	Autumn	Winter
CZUF	0.26	0.42	0.26	0.14	0.23	0.26	0.17	0.20
NUDZ	0.43	0.71	0.50	0.36	0.13	0.33	−0.02	−0.07
EPDZ	−0.67	−1.09	−0.73	−0.48	−0.33	−0.55	−0.12	−0.12

to the average LST of each functional zone. However, the area of the functional zone greatly affects the magnitude of the contribution index. Although the CZUF had the highest LST, it contributed little to the urban thermal environment because it had a small area. The NUDZ contributed the most to the urban thermal environment in the daytime. However the CZUF was the dominant contributor at night. For the NUDZ, the largest contribution was 0.71 in the summer daytime. The EPDZ had a constant negative contribution. However, the contribution of the EPDZ changed significantly in accordance with the growth of vegetation in different seasons. The cooling effect was the most obvious for flourishing vegetation in the EPDZ in the summer daytime, whereas the cooling effect was weaker in winter than in other seasons. When comparing the differences in the contributions to the regional thermal environment among the three zones during the daytime and nighttime, the contributions were smaller at nighttime than in daytime.

Through the analysis of regional contributions to the urban thermal environment, the role of each zone was determined. The NUDZ and CZUF were notable for their tremendously positive contributions to the regional thermal environment. It is necessary to further explore the formation mechanisms of the thermal environments in these two zones. By contrast, the EPDZ as a cooling source must be protected in future development. The cooling mechanism in the EPDZ should also be further analyzed to find ways to improve the thermal environments in the CZUF and NUDZ.

5.3. Landscape contributions to the urban thermal environment

5.3.1. Landscape contributions in the Core Zone of Urban Function

On the basis of the above analysis, the regional contributions to the urban thermal environment and the landscape components in each functional zone were calculated. To further compare the different mechanisms involved in the functional zones, the contribution of each landscape was calculated.

Urban land, forest, and cropland had the largest impact on the thermal environment in the CZUF (Fig. 5). Urban land as the main "source" contributed the most heat to the regional thermal environment in the daytime/nighttime in the different seasons. In particular, urban land made a maximum contribution to the regional thermal environment of 0.79 in the summer daytime. At the same time, the average LST of urban land was 1.30 °C higher than the regional average LST. There are four explanations for the high LST of urban land in the CZUF. First, the region is the political and cultural center of China and is clustered into three high-end industrial functional areas: the Zhongguancun national innovation demonstration zone, the Central Business District (CBD), and the Olympic central area. These areas have dense buildings and little vegetation. Second, the surface heat release efficiency is reduced because of reflection and absorption by the urban canopy. Third, there is less energy loss due to latent heat evaporation from the impervious urban surfaces. These three reasons explain why there is greater heat storage in urban surfaces. Fourth, anthropogenic heat sources are strong in the region. This phenomenon is distinct in the winter nighttime, when heating systems are used. A comparison of daytime and nighttime showed that the contribution of urban land to the thermal environment was slightly smaller in nighttime than in daytime, and the contribution in the nighttime was relatively stable in all seasons. However, there was a significant difference in the contribution of urban land to the regional thermal environment in the winter daytime, when urban land was an "urban cool island," decreasing the regional LST. The average LST of urban land was 0.08 °C lower than the regional average LST. Beijing is surrounded by mountains and has low wind speeds and dry air in the winter. Thus the potential for pollutant dispersion is weak in the vertical direction. With higher pollution levels (e.g., from heating systems, automobile exhausts), more atmospheric particles accumulate. These particles over the city further reduce incoming solar shortwave radiation and reduce the instability of the air near the ground. Atmospheric particulate levels near the ground then continue to increase, in a cycle of increasing pollution.

Cropland and forest lower the LSTs in the CZUF. The cropland contribution to the thermal environment was similar to that of forest but with some differences. The similarity between the two landscapes is consistent with their growing seasons. The cooling effect was strongest in the summer daytime, followed by spring and autumn. However, the negative contribution of forest was stronger than that of cropland in the daytime, and this phenomenon reversed in the nighttime (Fig. 6), mainly owing to the

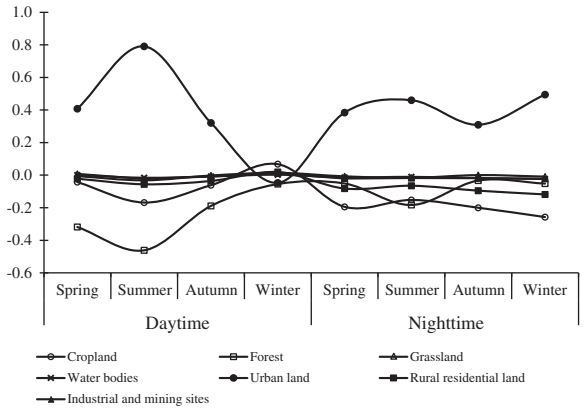

Fig. 5. Landscape contributions in the Core Zone of Urban Function.

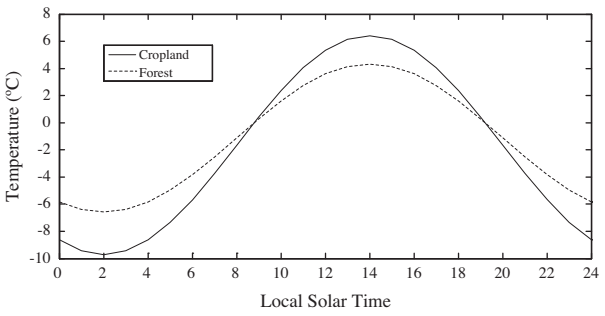

Fig. 6. Diurnal land surface temperatures of cropland and forest in winter in the Beijing metropolitan region.

Table 3
Landscape contributions in the New Urban Development Zone.

Landscapes	Daytime				Nighttime			
	Spring	Summer	Autumn	Winter	Spring	Summer	Autumn	Winter
Cropland	−0.28	−0.25	−0.08	0.02	−0.14	−0.13	−0.16	−0.16
Forest	0.01	−0.03	0	0.01	0	−0.01	0	0
Grassland	0	−0.02	−0.01	0	0	0	0	0
Water bodies	0.01	0	0	0	0	0	0	−0.01
Urban land	0.24	0.27	0.11	0	0.14	0.13	0.15	0.16
Rural residential land	0	0.02	−0.01	−0.01	0	0.01	0	0.01
Industrial and mining sites	0.04	0.04	0.01	−0.01	0.01	0.02	0.02	0.01

Table 4
Landscape contributions in the Ecological Preservation Development Zone.

Landscapes	Daytime				Nighttime			
	Spring	Summer	Autumn	Winter	Spring	Summer	Autumn	Winter
Cropland	0.42	0.31	0.21	0.12	−0.04	0.11	−0.14	−0.20
Forest	−0.65	−0.52	−0.32	−0.15	0.05	−0.23	0.19	0.32
Grassland	0.08	0.03	−0.02	−0.04	−0.06	−0.01	−0.08	−0.09
Water bodies	0.01	0.02	0.03	0.01	0.02	0.05	0.04	0.02
Urban land	0.06	0.09	0.05	0.03	0.03	0.04	0.02	0.01
Rural residential land	0.09	0.09	0.07	0.04	0.01	0.04	−0.01	−0.03
Industrial and mining sites	0.02	0.03	0.02	0.02	0.01	0.02	0	0

different thermal inertia of cropland and forest. Thermal inertia is defined as the ability to resist changes in the surface temperature (Carnahan and Larson, 1990),

$$P = \sqrt{\rho \cdot c \cdot K} \tag{2}$$

where P is the thermal inertia ($W\,s^{1/2}\,m^{-2}\,K^{-1}$), ρ is the density (kg/m^3), c is the specific heat of the material ($J\,kg^{-1}\,K^{-1}$), and K is the thermal conductivity ($J\,m^{-1}\,s^{-1}\,K^{-1}$). Sobrino and Kharraz (1999) indicated that thermal inertia increases from 500 $W\,s^{1/2}\,m^{-2}\,K^{-1}$ to 2500 $W\,s^{1/2}\,m^{-2}\,K^{-1}$ in accordance with a rising soil moisture content, and the thermal inertia of vegetation varies from 2000 $W\,s^{1/2}\,m^{-2}\,K^{-1}$ to 4200 $W\,s^{1/2}\,m^{-2}\,K^{-1}$. Fig. 6 shows an example of diurnal variations in winter, with a thermal inertia of 2700 $W\,s^{1/2}\,m^{-2}\,K^{-1}$ for cropland and 4200 $W\,s^{1/2}\,m^{-2}\,K^{-1}$ for forest (Sobrino and Kharraz, 1999).

LST can be simulated by using the approximate expression proposed by Price (1977):

$$\delta T(t) = J(t)\frac{\sin[\omega \cdot t - (\pi/4)]}{\omega^{1/2} \cdot P} \tag{3}$$

where $\delta T(t) = T(t) - T_{\min}$, t is time(s), $\omega = 2\pi/(24 \times 60 \times 60)s^{-1}$, and $J(t)$ is the surface net shortwave radiation calculated according to the following formula:

$$J(t) = SV(1-\alpha)(\sin\delta\sin\phi + \cos\delta\cos\phi\cos\Omega t) \tag{4}$$

where S is the solar constant (1368 w/m^2), V is the atmospheric transmittance in the visible spectrum (typically 0.75), α is the surface albedo, δ is the solar declination, ϕ is the latitude of observation, and Ωt is the diurnal phase of the sun with respect to local noon. To compare the surface albedos between cropland and forest, the albedo product on 2 December 2008 corresponding to the LST product was selected. The results indicated that in winter the mean surface albedo was 0.140 for cropland and 0.096 for forest. Finally, we calculated the diurnal LST variations in cropland and forest in winter (Fig. 6).

The LST of cropland was higher than that of forest in the daytime but lower at night (Fig. 6), showing that the LST of cropland changes faster than that of forest. It can be inferred from Eq. (3) that thermal inertia was a significant cause of the diurnal LST variations. The thermal inertia of cropland was far smaller than that of forest; thus, the LST of cropland changed more readily than that of forest, which explains the diurnal change in the roles of cropland and forest.

Grass and water bodies contributed negatively to the regional thermal environment. Rural residential land and industrial and mining sites both contributed negatively to the regional thermal environment, mainly because the urban land area was large and the LST of urban land was much higher than for the other landscapes. The average LSTs of rural residential land and industrial and mining sites were also higher than those of vegetation and water bodies.

5.3.2. Landscape contributions in the New Urban Development Zone

Urban land and cropland played major roles in the urban thermal environment of the NUDZ (Table 3). Compared to the CZUF, the positive contribution of urban land was lower, the cooling effect of forest was lower, and the negative contribution of cropland was increased. This zone also differed in terms of its landscape composition. Only 11% of the land was urban. The dominant landscape was cropland (60.1%), and forest covered only 3.6% of the zone. Industrial and mining sites also made relatively higher contributions to the thermal environment in the NUDZ. Urban land, rural residential land, and industrial and mining sites in summer daytime made the largest contributions to the thermal environment. Such contributions were found to be more consistent in the nighttime than in the daytime.

5.3.3. Landscape contributions in the Ecological Preservation Development Zone

Cropland and forest had major roles in the urban thermal environment of the EPDZ (Table 4). There was a distinct difference between the EPDZ and the two central zones. The contribution of urban land to the thermal environment was substantially less than in the two central zones. In addition, the roles of cropland and forest differed between the daytime and nighttime. During the daytime, cropland was the main contributor to increasing the regional LST, whereas forest was the main source of cooling. In contrast, at night the forest LST was notably higher than the regional average LST. Cropland and grassland were the main sources of

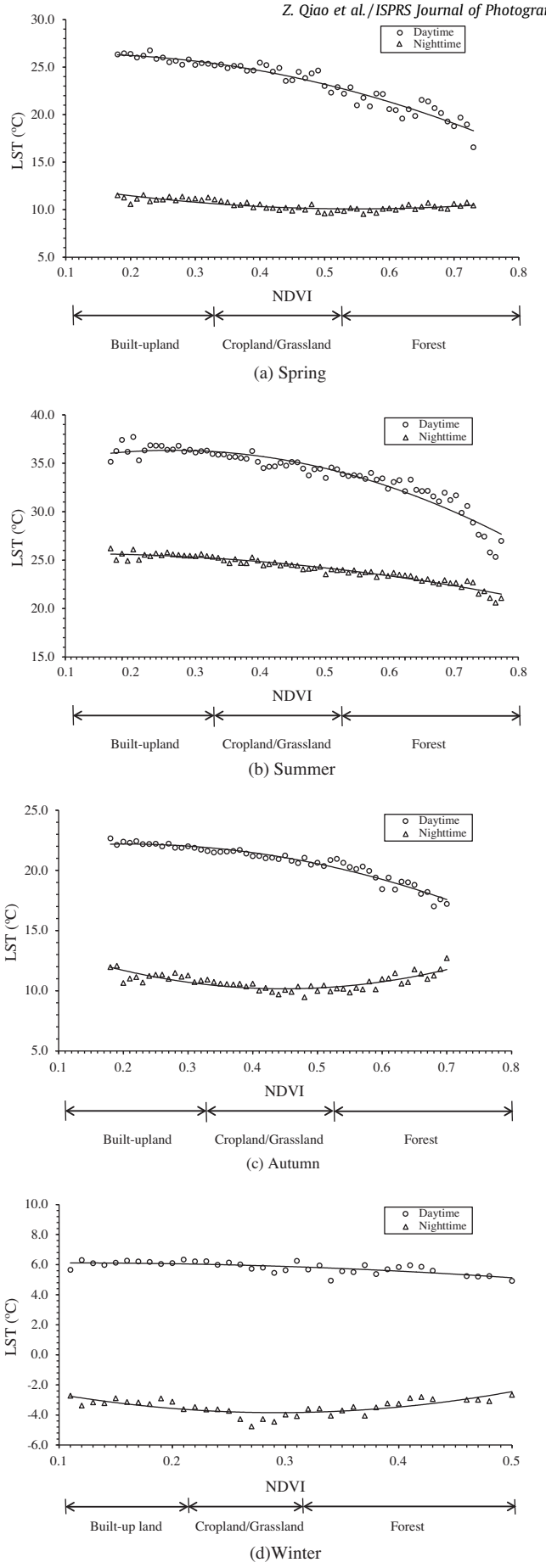

Fig. 7. The LST–NDVI relationship, averaged by the NDVI for 0.01 intervals.

Table 5
Regression parameters between LST and NDVI in different seasons.

Time	Daytime	Nighttime
Spring	LST = −21.12 $NDVI^2$ + 4.705 NDVI + 26.12 R^2 = 0.933	LST = 11.44 $NDVI^2$ − 12.54 NDVI + 13.52 R^2 = 0.678
Summer	LST = −25.71 $NDVI^2$ + 14.89 NDVI + 34.18 R^2 = 0.911	LST = −7.157 $NDVI^2$ + 1.525 NDVI + 25.58 R^2 = 0.935
Autumn	LST = −18.86 $NDVI^2$ + 7.746 NDVI + 21.39 R^2 = 0.947	LST = 24.98 $NDVI^2$ − 22.36 NDVI + 15.16 R^2 = 0.642
Winter	LST = −6.531 $NDVI^2$ + 1.460 NDVI + 6.030 R^2 = 0.543	LST = 32.64 $NDVI^2$ − 19.12 NDVI − 1.043 R^2 = 0.562

regional LST cooling in the nighttime. As mentioned above, differences in thermal inertia generated the diurnal LST differences.

5.4. Relationship between LST and NDVI

The above analyses clearly indicate the relationship between landscapes and the temporal-spatial pattern of LST in the study region. However, heterogeneity existed even within the same type of landscape. Therefore, the same landscape could make different contributions to the overall thermal environment. The NDVI can be used to determine LST variations in the same land use/cover type, and previous studies have suggested a strong negative relationship between LST and NDVI (Carlson et al., 1994; Dousset and Gourmelon, 2003). We investigated diurnal or seasonal differences in this relationship using MODIS images with high temporal resolution. We reclassified the pixels of index values at intervals of 0.01 and then averaged the LST of the corresponding pixels. Considering the population trends and the landscape percentages in the CZUF, we evaluated the LST-NDVI relationship for four seasons in the CZUF (Fig. 7).

The regression parameters are shown in Table 5. Significant correlations between the LST and NDVI were found. The LST and NDVI in summer had the strongest negative correlation. LST decreased with rising NDVI in the daytime/nighttime indicating that vegetation had a notable cooling effect during summer. Similar phenomena appeared in the daytime during the other seasons. However, the opposite was true in the nighttime, except in summer. During nighttime in the spring, autumn, and winter, the LST was highest in the built-up areas, displaying a downward trend from built-up land to cropland/grassland but an increasing trend with the rising vegetation index from cropland/grassland to forest. On the basis of the calculated regression parameters, the turning points of NDVI that led to a change in LST were 0.548, 0.448, and 0.293 in spring, summer, and autumn, respectively. This confirms that forest had a higher LST than cropland in the nighttime because of difference in their thermal inertias, as discussed above. It is thus reasonable to assume that dense vegetation would increase the LST in the winter nighttime in the metropolitan region, while having a notable cooling effect in summer.

6. Discussion and conclusions

This study proposed a contribution index to evaluate the contributions of different zones and landscapes to the urban thermal environment. With the superior temporal resolution of MODIS LST products, the mechanisms involved in generating the urban thermal environment in the daytime and nighttime during different seasons could be explored.

The functional zones played different roles in the urban thermal environment in the Beijing metropolitan region because of differences in their landscapes. The average LSTs of the CZUF and NUDZ were higher than in the Beijing metropolitan region in the daytime, but seasonal fluctuations generated a decrease in these contributions in nighttime. CZUF had the largest average LST among the three zones because of its high percentage of urban land (61%). However, the CZUF contributed less than the NUDZ to the regional thermal environment because the CZUF only accounts for 8.5% of the area of the Beijing metropolitan region. Overall, the two zones were the main sources of the rise in the regional LST. Careful attention should be paid to the urban development of these two zones to improve the regional thermal environment. The EPDZ made a negative contribution at all times because of its dense vegetation and high elevation. The negative contribution was largest in the summer daytime and reached a minimum in the winter nighttime, in accordance with the growth of deciduous vegetation.

Landscapes had different roles during the daytime and nighttime in the different seasons and in different regions. Urban land was the most important "source" of heat in the urban thermal environment. The contribution of urban land was much larger in the summer daytime than in other seasons, which led to the strongest UHI effect in the Beijing metropolitan region occurring in the summer daytime. However, the seasonal fluctuations of this contribution were stabilized in the nighttime. The results further indicated that solar shortwave radiation was the most important factor for determining the urban thermal environment, and anthropogenic heat releases, which increase the urban LST, have remained relatively stable. There was a particular phenomenon associated with urban land in the winter daytime. The contribution of urban land to the regional thermal environment was −0.05 in the CZUF in the winter daytime, which generated an average LST that was −0.08 °C lower than the regional LST. There was an urban cool island in winter because atmospheric particles reduced the incoming solar shortwave radiation. The urban cool island reduced the instability of air near the ground and further increased the accumulation of atmospheric particles, which led to increased levels of urban air pollution in winter.

The roles of cropland and forest produced an inter-conversion during the daytime and nighttime. This phenomenon was most distinct in the EPDZ, which was the zone with the least urban land. The dominant landscape was forest (63.5%), followed by cropland (16.7%). Cropland was the main contributor to the regional thermal environment in terms of daytime LST increases. By contrast, forest had a large negative role in the regional LST. This condition was reversed during the night. The thermal inertia of cropland was far smaller than that of forest; thus, the LST of cropland changed more readily than that of forest, which explains the diurnal change in the roles of cropland and forest.

Through quantitative evaluation of the LST-NDVI relationships during the four seasons in the CZUF, we further verified the reliability of the contributions of different landscapes to the regional thermal environment. This study revealed diurnal and seasonal differences in the LST–NDVI relationship. The strongest negative correlation between LST and NDVI occurred in summer. However, the opposite was true in the nighttime, except in summer. When the NDVI reached 0.548, 0.448, and 0.293 in the nighttime of spring, summer, and autumn respectively, the LSTs clearly changed. This result illustrates that dense vegetation has a heat preservation effect during the nighttime. Vegetation partitions may thus be an effective approach to regulating the thermal environments of cities.

Several topics require further investigation. First, the contribution of water bodies to the regional LST was not apparent in this study because of the low resolution of MODIS (1 km). The LST retrieval images need to be improved to increase the spatial resolution of pixels, and an algorithm of multi-source image fusion should be developed to increase the temporal resolution. Second, dynamical research regarding the effects of urbanization on the urban thermal environment needs to be undertaken. Third, it is necessary to investigate the effects of human activities on the urban thermal environment in landscapes in different regions to further understand the contributions of different landscapes to the urban thermal environment.

Acknowledgment

This study was supported by National Key Technology R&D Program of China during the Twelfth Five-Year Plan Period (2012BAC13B01) and the project of National Natural Science Foundation of China under Grant 41071357.

References

Ash, C., Jasny, B.R., Roberts, L., Stone, R., Sugden, A.M., 2008. Reimagining cities. Science 319 (5864), 739.
Beijing Statistics Bureau, 2010. Beijing Statistical Yearbook 2010. China Statistics Press, Beijing.
Carlson, T.N., Gillies, R.R., Perry, E.M., 1994. A method to make use of thermal infrared temperature and NDVI measurements to infer surface soil water content and fractional vegetation cover. Remote Sensing Reviews 9, 161–173.
Carnahan, W.H., Larson, R.C., 1990. An analysis of an urban heat sink. Remote Sensing of Environment 33 (1), 65–71.
Chen, X.L., Zhao, H.M., Li, P.X., Yin, Z.Y., 2006. Remote sensing image-based analysis of the relationship between urban heat island and land use/cover changes. Remote Sensing of Environment 104 (2), 133–146.
Christen, A., Voogt, R., 2004. Energy and radiation balance of a central European city. International Journal of Climatology 24 (11), 1395–1421.
Dousset, B., Gourmelon, F., 2003. Satellite multi-sensor data analysis of urban surface temperatures and landcover. ISPRS Journal of Photogrammetry and Remote Sensing 58, 43–54.
Friedl, M.A., Sulla-Menashe, D., Tan, B., 2010. MODIS Collection 5 global land cover: algorithm refinements and characterization of new datasets. Remote Sensing of Environment 114 (1), 168–182.
Gallo, K.P., McNab, A.L., Karl, T.R., Brown, J.F., Hood, J.J., Tarpley, J.D., 1993. The use of a vegetation index for assessment of the urban heat island effect. International Journal of Remote Sensing 14 (11), 2223–2230.
Gallo, K.P., Owen, T.W., 1998. Assessment of urban heat Islands: a multi-sensor perspective for the Dallas-Ft. worth, USA region. Geocarto International 13 (4), 35–41.
Hawkins, T.W., Brazel, A.J., Stefanov, W.L., Bigler, W., Saffell, E.M., 2004. The role of rural variability in urban heat island determination for Phoenix, Arizona. Journal of Applied Meteorology 43 (3), 476–486.
Hung, T., Uchihama, D., Ochi, S., Yasuoka, Y., 2006. Assessment with satellite data of the urban heat island effects in Asian mega cities. International Journal of Applied Earth Observation and Geoinformation 8 (1), 34–48.
Jin, M., Dickinson, R.E., Zhang, D., 2005. The footprint of urban areas on global climate as characterized by MODIS. Journal of Climate 18 (10), 1551–1565.
Jones, P.D., Groisman, P.Y., Coughlan, M., Plummer, N., Wang, W.C., Karl, T.R., 1990. Assessment of urbanization effects in time series of surface air temperature over land. Nature 347 (6289), 169–172.
Kalnay, E., Cai, M., 2003. Impact of urbanization and land-use change on climate. Nature 423 (6939), 528–531.
Kondoh, A., Nishiyama, J., 2000. Changes in hydrological cycle due to urbanization in the suburb of Tokyo Metropolitan area, Japan. Advances in Space Research 26 (7), 1173–1176.
Liang, S.L., Fang, H.L., Chen, M.Z., Shuey, C.J., Walthall, C., Daughtry, C., Morisette, J., Schaaf, C., Strahler, A., 2002. Validating MODIS land surface reflectance and albedo products: methods and preliminary results. Remote Sensing of Environment 83 (1–2), 149–162.
Liu, J.Y., Liu, M.L., Tian, H.Q., 2005. Spatial and temporal patterns of China's cropland during 1990–2000: an analysis based on Landsat TM data. Remote Sensing of Environment 98 (4), 442–456.
Lucht, W., Hyman, A.H., Strahler, A.H., Barnsley, M.J., Hobson, P., Muller, J.-P., 2000. A comparison of satellite-derived spectral albedos to ground-based broadband albedo measurements modelled to satellite spatial scale for a semi-desert landscape. Remote Sensing of Environment 74, 85–98.
Nichol, J., Wong, M.S., 2005. Modeling urban environmental quality in a tropical city. Landscape and Urban Planning 73 (1), 49–58.
Oke, T.R., 1973. City size and the urban heat island. Atmospheric Environment 7 (8), 769–779.
Oke, T.R., 1982. The energetic basis of the urban heat island. Quarterly Journal of the Royal Meteorological Society 108 (445), 1–24.
Oke, T.R., 1988. The urban energy balance. Progress in Physical Geography 12 (4), 471–508.
Parker, D.E., 2004. Climate: large-scale warming is not urban. Nature 432 (7015), 290-290.

Pongracz, R., Bartholy, J., Dezso, Z., 2006. Remotely sensed thermal information applied to urban climate analysis. Advances in Space Research 37 (12), 2191–2196.
Price, J.C., 1977. Thermal inertia mapping: a new view of the earth. Journal of Geophysical Reasearch 82 (18), 2582–2590.
Rajasekar, U., Weng, Q., 2009. Urban heat island monitoring and analysis using a non-parametric model: a case study of Indianapolis. ISPRS Journal of Photogrammetry and Remote Sensing 64 (1), 86–96.
Rao, P.K., 1972. Remote sensing of urban "heat islands" from an environmental satellite. Bulletin of the American Meteorological Society 53, 647–648.
Rizwan, A.M., Dennis, Y.C., Liu, C., 2008. A review on the generation, determination and mitigation of Urban Heat Island. Journal of Environmental Sciences 20 (1), 120–128.
Schaaf, C.B., Gao, G., Strahler, A.H., Lucht, W., Li, X., Tsang, T., Strugnell, N.C., Zhang, X., Jin, Y., Muller, J.P., Lewis, P., Barnsely, M.J., Hobson, P., Disney, M., Roberts, G., Dunderdale, M., Doll, C., D'Entremont, R.P., Hu, B., Liang, S., Privette, J., Roy, D.P., 2002. First operational BRDF, Albedo and Nadir reflectance products from MODIS. Remote Sensing of Environment 83 (1–2), 135–148.
Sobrino, J.A., Kharraz, M.H.E., 1999. Combining afternoon and morning NOAA satellites for thermal inetia estimation: 1. Algorithm and its testing with Hydrologic Atmospheric Pilot Experiment-Sahel data. Journal of Geophysical Research: Atmospheres 104, 9445–9454.
Streutker, D.R., 2002. A remote sensing study of the urban heat island of Houston, Texas. International Journal of Remote Sensing 23 (13), 2595–2608.
Trusilova, K., Jung, M., Churkina, G., Karstens, U., Heimann, M., Claussen, M., 2008. Urbanization impacts on the climate in Europe: numerical experiments by the PSU–NCAR Mesoscale Model (MM5). Journal of Applied Meteorology and Climatology 47 (5), 1442–1455.
van Leeuwen, W.J.D., Huete, A.R., Laing, T.W., 1999. MODIS vegetation index compositing approach: a prototype with AVHRR data. Remote Sensing of Environment 69 (3), 264–280.
Voogt, J.A., Oke, T.R., 2003. Thermal remote sensing of urban climates. Remote Sensing of Environment 86 (3), 370–384.
Wan, Z., Zhang, Y.L., Zhang, Q.C., Li, Z.L., 2004. Quality assessment and validation of the MODIS global land surface temperature. International Journal of Remote Sensing 25 (1), 261–274.
Wan, Z., Dozier, J., 1996. A generalized split-window algorithm for retrieving land-surface temperature from space. IEEE Transactions on Geoscience and Remote Sensing 34 (4), 892–905.
Wang, K., Liu, J., Zhou, X., Sparrow, M., Ma, M., Sun, Z., Jiang, W., 2004. Validation of the MODIS global land surface albedo product using ground measurements in a semi-desert region on the Tibetan Plateau. Journal of Geophysical Research Atmospheres 109, 1–9.
Wang, K., Wang, J., Wang, P., Sparrow, M., Yang, J., Chen, H., 2007. Influences of urbanization on surface characteristics as derived from the Moderate-Resolution Imaging Spectroradiometer: a case study for the Beijing metropolitan region. Journal of Geophysical Research Atmospheres 112, 1–12.
Weng, Q., 2001. A remote sensing-GIS evaluation of urban expansion and its impact on surface temperature in the Zhujiang Delta, China. International Journal of Remote Sensing 22 (10), 1999–2014.
Wood, F., 1988. Comment: on the need for validation of the Jones et al. temperature trends with respect to urban warming. Climatic Change 12 (3), 297–312.
Xia, X.A., Chen, H.B., Wang, P.C., 2006. Variation of column-integrated aerosol properties in a Chinese urban region. Journal of Geophysical Research: Atmospheres 118 (13), 6869–7425.
Xu, S., 2009. An approach to analyzing the intensity of the daytime surface urban heat island effect at a local scale. Environmental Monitoring and Assessment 151 (1–4), 289–300.
Yuan, F., Bauer, M.E., 2007. Comparison of impervious surface area and normalized difference vegetation index as indicators of surface urban heat island effects in Landsat imagery. Remote Sensing of Environment 106 (3), 375–386.
Zhang, J.H., Hou, Y.Y., Li, G.C., Yan, H., Yang, L.M., Yao, F.M., 2005. The diurnal and seasonal characteristics of urban heat island variation in Beijing city and surrounding areas and impact factors based on remote sensing satellite data. Science in China Series D-Earth Sciences 48, 220–229.